

## Chapter

# Contribution to the Calculation of Physical Properties of BeSe Semiconductor

*Mohamed Amine Ghebouli and Brahim Ghebouli*

## Abstract

We expose various physical parameters of binary compound BeSe in the stable zinc blend and NiAs structures using the functional HSE hybrid, GGA-PBE, and LDA. We deduce elastic constants, mechanical parameters, and wave velocities according to different orientations. BeSe semiconductor has  $\Gamma$ -X (2.852 eV) and  $\Gamma$ -K (0.536 eV) bandgap in zinc blend and NiAs structures. Electrons transit from Se-p site to the Be-s state and show covalent bonding. Optical absorption peaks result from electronic transitions under ultraviolet light irradiation.

**Keywords:** CASTEP, zinc blend, NiAs, band structure, bandgap, absorption, BeSe

## 1. Introduction

Researchers have focused on II-VI semiconductors, which are intended for technological applications. BeSe crystallizes in zinc blend structure at room temperature and its properties depend on structure, pressure, temperature, and calculation method. The HSE hybrid underestimates the lattice parameters compared to GGA-PBE and LDA but gives a bandgap in accordance with the experimental value. The phonon dispersion curve of BeSe shows two optical and acoustic couplets and confirms its stability. The maximum of reflectivity (63% and 56%) is observed in the ultraviolet light domain. We expose the detailed calculation concerning the lattice parameters, elastic constants, bandgap, phonons frequencies, and optical parameters. For works carried out by other researchers, we note the transition from zinc blend phase to NiAs structure at 55 GPa [1]. The study of elastic constants and bandgap of BeSe in zinc blend phase [2, 3], the experimental bandgap ranging from 2 eV to 4.5 eV [4, 5], a small ionic radius ratio, a high degree of covalent bonding, and high hardness [6]. Appropriate bandgap and optical absorption parameters make BeSe as an important material in the area of catalysis and luminescent devices [7–9].

## 2. Computational method

We perform calculations on BeSe by using the CASTEP code [10]. The energy  $E_{\text{cut}}$  of 660 eV and k-points of  $8 \times 8 \times 8$  using Monkhorst-Pack scheme [11] ensure well

convergence. We use  $20 \times 20 \times 20$  k-points in the computation of optical parameters. The GGA, LDA, and HSE hybrid functional [12, 13] treat the exchange-correlation potential. Broyden-Fletcher-Goldfarb-Shanno (BFGS) minimization technique [14] determines the structural parameters. The tolerance of geometry optimization was a total energy  $5 \times 10^{-6}$  eV/atom, maximum ionic Hellmann-Feynman force  $0.01$  eV/Å, and maximum stress  $0.02$  eV/Å<sup>3</sup>.

### 3. Results and discussions

#### 3.1 Ground state

The position of Be atom is the corner (0, 0, 0), while the Se atom takes place at (1/4, 1/4, 1/4) and (1/3, 2/3, 1/4) for zinc blend and NiAs phases. **Figure 1(a)** gives

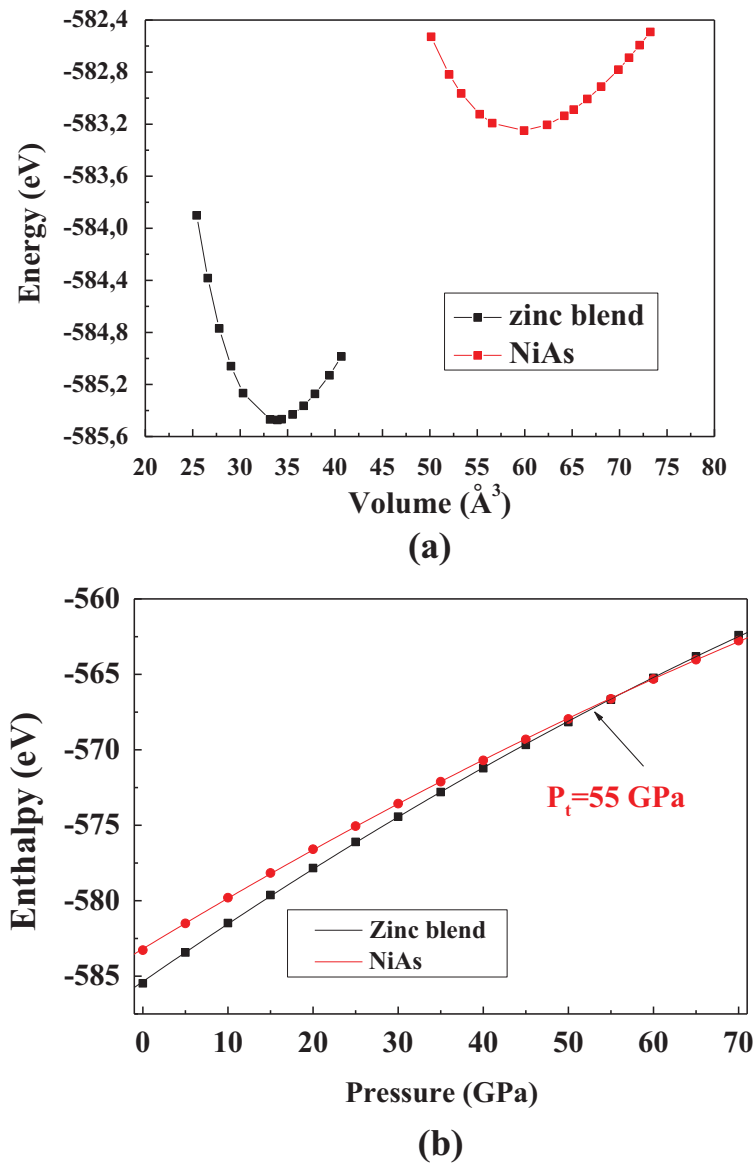


**Figure 1.** The plots of total energy versus volume (a) and enthalpy versus pressure (b) for BeSe in zinc blend and NiAs phases.

|             | Zinc blend |       |            |            |  | NiAs  |        |            |     |  |
|-------------|------------|-------|------------|------------|--|-------|--------|------------|-----|--|
|             | GGA        | LDA   | HSE hybrid | Exp        | Other                                  | GGA   | LDA    | HSE hybrid | Exp | Other                                  |
| $a$ (Å)     | 5.129      | 5.083 | 4.976      | 5.139 [15] | 5.137 [16]<br>5.037 [17]<br>5.087 [18] | 3.513 | 3.456  | 3.415      |     | 3.524 [16]<br>3.421 [17]<br>3.502 [19] |
| $c$ (Å)     |            |       |            |            |  | 5.459 | 5.461  | 5.347      |     | 5.462 [16]<br>5.398 [17]<br>5.529 [19] |
| $B_0$ (GPa) | 74.50      | 87.35 | 99.484     | 92.20 [15] | 74.97 [18]<br>80 [4]<br>96.5 [20]      | 89.20 | 100.30 | 112.76     |     | 94.7 [17]<br>86 [21]<br>109.6 [22]     |
| $B'$        | 3.82       | 3.65  | 3.565      |            | 4.02 [23]<br>3.58 [24]<br>3.85 [19]    | 3.94  | 3.826  | 3.749      |     | 3.852 [17]<br>3.70 [25]                |

**Table 1.** Lattice parameters, bulk modulus, and its pressure derivative for BeSe in zinc blend and NiAs structures within GGA-PBE, LDA, and HSE hybrid functional.

the plots of total energy versus unit cell volume, where the zinc blend phase is more stable. **Figure 1(b)** visualizes the effect of pressure on formation enthalpy. The two enthalpy-pressure diagrams show a transition region around 55 GPa [1]. We report in **Table 1** that the lattice parameters, bulk modulus, and its pressure derivative are calculated with GGA, LDA, and HSE hybrid. Our results agree well with experimental measurements [15] and theoretical data [4, 16–25]. The HSE hybrid underestimates the lattice parameters.

### 3.2 Elastic constants and mechanical parameters

**Table 2** includes elastic moduli of BeSe in both phases within GGA and LDA. Our elastic constants of zinc blend structure agree with theoretical values [18, 22, 26, 27]. The following relationships [28, 29] ensure the elastic stability of BeSe.

Zinc blend

$$0 < C_{11} + 2C_{12}, 0 < C_{44}, 0 < C_{11} - C_{12}, C_{12} < B < C_{11} \quad (1)$$

NiAs

$$0 < C_{11} - |C_{12}|, 0 < C_{33}(C_{11} + C_{12}) - 2C_{13}^2, 0 < C_{44} \quad (2)$$

**Figure 2** shows the dependence of elastic moduli on pressure for beryllium selenide in zinc blend and NiAs phases. We list in **Table 2** the bulk modulus, shear modulus, Young’s modulus, Poisson’s ratio, anisotropy factor, and  $B_H/G_H$  ratio. The Poisson’s ratio and anisotropy factor indicate the covalent bonding and strong anisotropy in BeSe. The reported  $B_H/G_H$  value translates the brittle zinc blend phase and ductile NiAs structure. **Figure 3** visualizes the effect of orientation on Poisson’s ratio (a) and shear modulus (b) in xy, xz, and yz planes. It can be seen that the two parameters are isotropic only in the B8 phase and in the xy plane. **Table 3** predicts the maximum and minimum values of Young’s modulus, linear compressibility, shear

|                | Zinc blend |        |                       | NiAs       |        |       |
|----------------|------------|--------|-----------------------|------------|--------|-------|
|                | GGA        | LDA    | Other                 | GGA        | LDA    |       |
| $C_{11}$ (GPa) | 120.06     | 137.22 | 117 [18]<br>145 [24]  | 140.27     | 167.04 |       |
| $C_{12}$ (GPa) | 30.73      | 55.94  | 45.5 [26]<br>51 [22]  | 71.51      | 80.20  |       |
| $C_{44}$ (GPa) | 66.2       | 74.35  | 73.39 [26]<br>61 [22] | 8.48       | 14.57  |       |
| $C_{13}$ (GPa) |            |        |                       | 36.45      | 46.51  |       |
| $C_{33}$ (GPa) |            |        |                       | 178.40     | 202.79 |       |
| $\Theta_D$ (K) | 460.91     | 465.77 | 407 [26]              | 280.75     | 332.74 |       |
| $B$ (GPa)      | $B_V$      | 60.51  | 83.08                 | 83.08      | 98.15  |       |
|                | $B_R$      | 60.51  | 83.08                 | 83.08      | 98.15  |       |
|                | $B_H$      | 60.51  | 83.08                 | 83.08      | 98.14  |       |
| $G$ (GPa)      | $G_V$      | 131.16 | 60.86                 | 66.24 [27] | 31.23  | 60.86 |
|                | $G_R$      | 127.51 | 55.83                 | 61.14 [27] | 16.22  | 55.83 |
|                | $G_H$      | 129.34 | 58.53                 | 63.78 [27] | 23.73  | 58.53 |
| $E_H$ (GPa)    | 129.34     | 141.82 | 153.42 [27]           | 65.00      | 86.89  |       |
| $\sigma_H$     | 0.138      | 0.21   | 0.203 [27]            | 0.36       | 0.35   |       |
| $A^U$          | 0.188      | 0.45   |                       | 4.62       | 2.60   |       |
| $B_H/G_H$      | 0.46       | 1.41   | 1.349 [27]            | 3.5        | 3.05   |       |

**Table 2.**

Elastic constants  $C_{ij}$ , Debye temperature  $\Theta_D$ , bulk modulus  $B$ , shear modulus  $G$ , Young's modulus  $E_H$ , Poisson's ratio  $\sigma_H$ , anisotropy factor  $A^U$  and ratio  $B_H/G_H$  for BeSe in zinc blend and NiAs structures.

modulus, and Poisson's ratio. **Table 2** reports the Debye temperature of BeSe, which agrees with the theoretical value [26]. **Table 4** predicts elastic wave velocities along [100], [110], [111], and [001] directions.

### 3.3 Electronic parameters

**Figure 4** shows the band structure of BeSe using GGA-PBE and HSE hybrid functional. We observe the indirect bandgap  $\Gamma$ -X ( $\Gamma$ -K) in the zinc blend (NiAs) structure. **Table 5** reports the bandgap between various symmetry points. The bandgap of BeSe in the zinc blend structure agrees with other calculations [3, 16, 23, 31]. **Figure 5** displays the dependence on the pressure of the direct and indirect bandgap. The bandgap calculated using the HSE hybrid agrees with the experimental one [3, 32, 33]. **Figure 6** shows the plots of total and partial densities of states. Se-p and Be-s orbitals are responses for the upper valence band. The first conduction band is wider for both structures and consists of Be-s and Se-p orbitals, with a small contribution of the Se-s site. The optical transition occurs from Se-p state to the Be-s site. There is a hybridization between Se-p and Be-s in the upper valence band, which translates their covalent bonding.

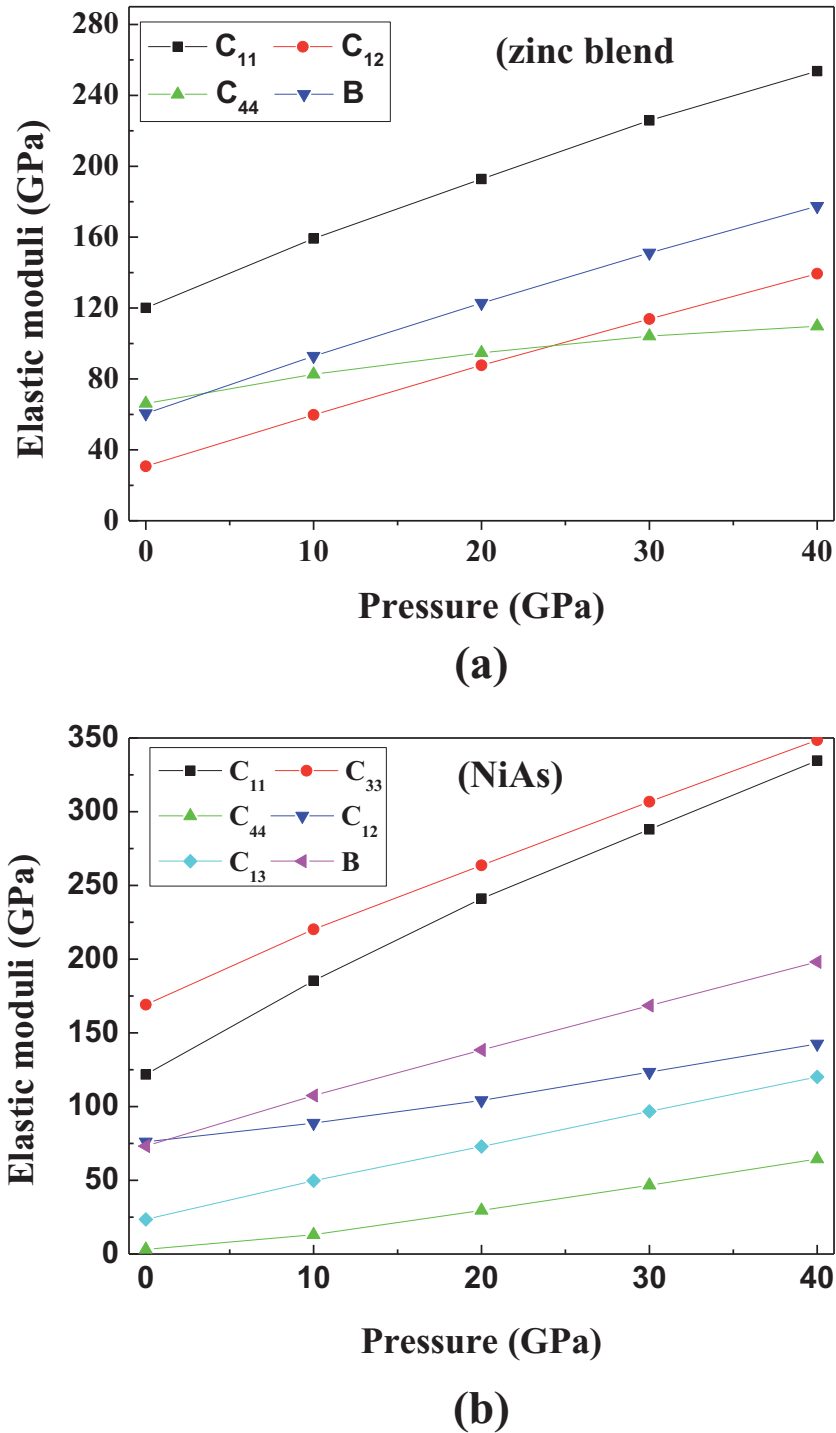


**Figure 2.**  
 Elastic moduli versus pressure in zinc blend (a) and NiAs (b) phases.

### 3.4 Phonon frequencies

Figure 7 shows the phonon dispersion curve of BeSe in zinc blend structure. Optical (acoustic) phonons exhibit two couplets of longitudinal optical (LO)

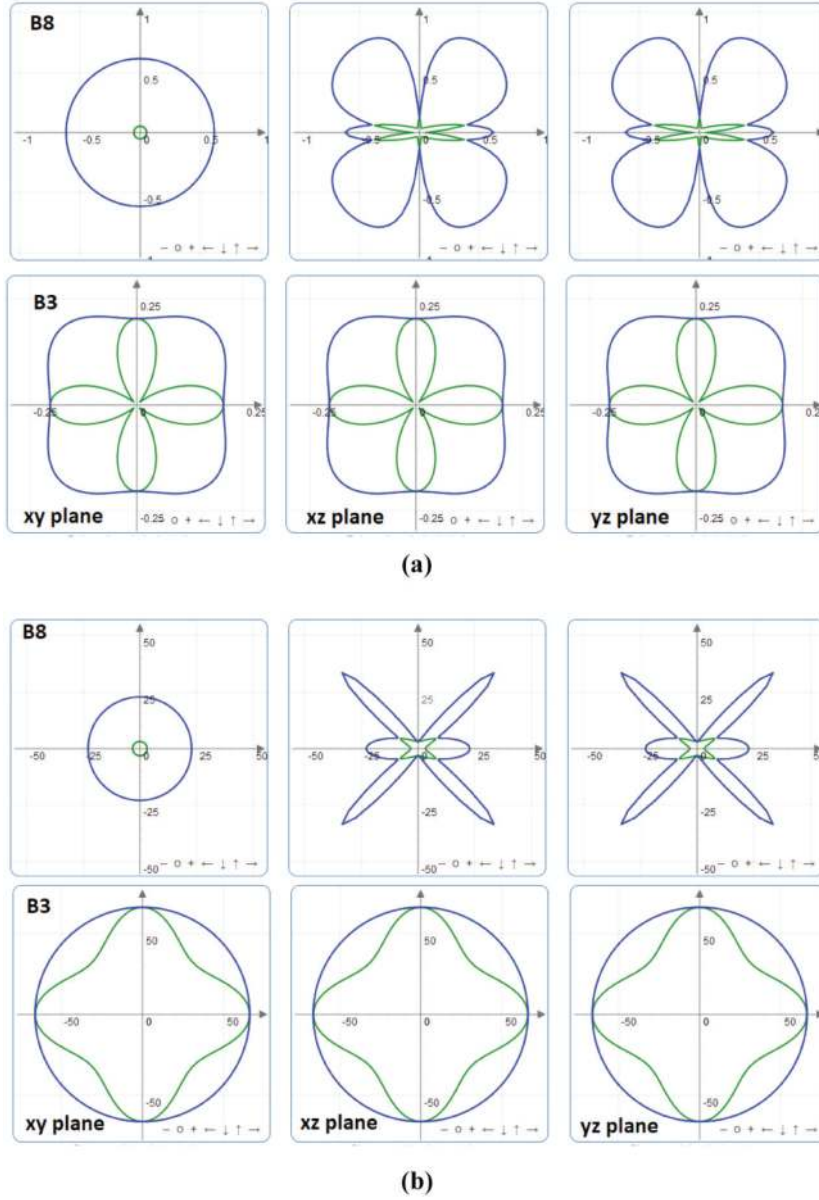


**Figure 3.** The orientation effect on Poisson's ratio (a) and shear modulus (b) in zinc blend and NiAs phases.

| Parameters |     | Young's modulus |           | Linear compressibility |               | Shear modulus |           | Poisson's ratio |                |
|------------|-----|-----------------|-----------|------------------------|---------------|---------------|-----------|-----------------|----------------|
|            |     | $E_{min}$       | $E_{max}$ | $\beta_{min}$          | $\beta_{max}$ | $G_{min}$     | $G_{max}$ | $\sigma_{min}$  | $\sigma_{max}$ |
| Zinc blend | GGA | 107.54          | 145.55    | 5.5083                 | 5.5083        | 44.665        | 44.665    | 0.009           | 0.253          |
|            | LDA | 104.83          | 171.79    | 4.0142                 | 4.0142        | 40.644        | 74.354    | 0.0039          | 0.409          |
| NiAs       | GGA | 42.108          | 163.56    | 4.5012                 | 4.5012        | 13.201        | 47.33     | 0.118           | 0.623          |
|            | LDA | 49.954          | 185.29    | 3.3662                 | 3.3662        | 14.575        | 64.941    | 0.102           | 0.719          |

**Table 3.** The maximum and minimum values of Young's modulus  $E$ , linear compressibility  $\beta$ , shear modulus  $G$ , and Poisson's ratio  $\sigma$  for BeSe in zinc blend and NiAs structures.

| Material   | Directions                    | [100] | [110] | [111] | [001] |
|------------|-------------------------------|-------|-------|-------|-------|
| Zinc blend | $v_1$ ( $\text{ms}^{-1}$ )    | 5439  | 5898  | 6043  | —     |
|            | $v_{t1}$ ( $\text{ms}^{-1}$ ) | 3803  | 4305  | 3316  | —     |
|            | $v_{t2}$ ( $\text{ms}^{-1}$ ) | 3803  | 3803  | 3316  | —     |
| NiAs       | $v_1$ ( $\text{ms}^{-1}$ )    | 5192  | —     | —     | 6067  |
|            | $v_{t1}$ ( $\text{ms}^{-1}$ ) | 2187  | —     | —     | 1243  |
|            | $v_{t2}$ ( $\text{ms}^{-1}$ ) | 1243  | —     | —     | 1243  |

**Table 4.**  
 Sound velocities for BeSe along with main directions in zinc blend and NiAs structures.

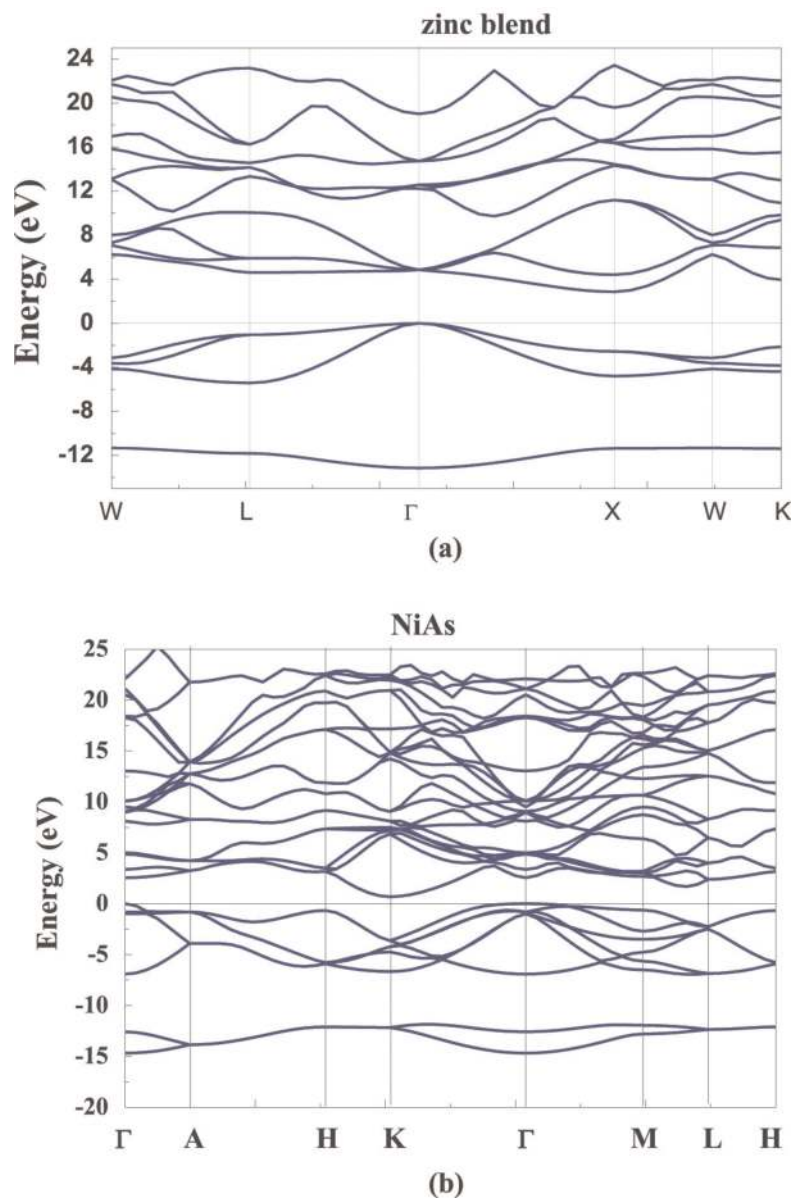


**Figure 4.**  
 The band structure of BeSe in zinc blend (a) and NiAs (b) phases at various points in the Brillouin zone.

|                          | Zinc blend |       |            |                      |                        | NiAs |      |            |
|--------------------------|------------|-------|------------|----------------------|------------------------|------|------|------------|
|                          | GGA        | LDA   | HSE hybrid | Exp                  | Other                  | GGA  | LDA  | HSE hybrid |
| $E_{\Gamma-\Gamma}$ (eV) | 4.84       | 4.42  | 5.81       | 4.72 [3]<br>5.5 [30] |                        | 2.55 | 2.43 | 3.45       |
| $E_{L-L}$ (eV)           | 5.65       | 5.52  | 7.40       |                      |                        | 4.64 | 4.88 | 6.02       |
| $E_{X-X}$ (eV)           | 5.41       | 5.20  | 6.71       |                      |                        |      |      |            |
| $E_{\Gamma-X}$ (eV)      | 2.85       | 2.408 | 3.45       | 4-4.5 [3]            | 2.41 [31]<br>3.12 [16] |      |      |            |
| $E_{\Gamma-L}$ (eV)      | 4.60       | 4.39  | 6.05       |                      | 4.33 [23]              | 2.38 | 2.27 | 6.23       |
| $E_{\Gamma-K}$ (eV)      | 3.94       | 3.62  | 4.71       | 4.73 [32]            |                        | 0.68 | 0.51 | 1.16       |
| $E_{M-M}$ (eV)           |            |       |            |                      |                        | 3.28 | 2.98 | 3.94       |

**Table 5.**  
Band gaps for BeSe at equilibrium between various symmetry points in zinc blend and NiAs structures.

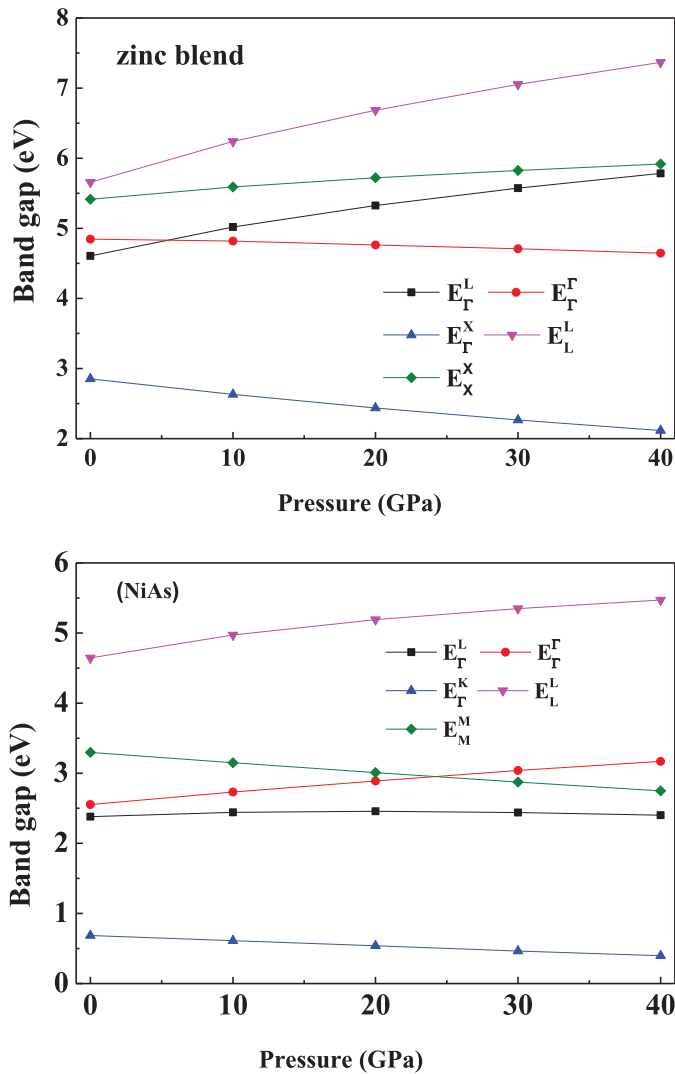


**Figure 5.**  
The band gaps versus pressure in zinc blend and NiAs phases.



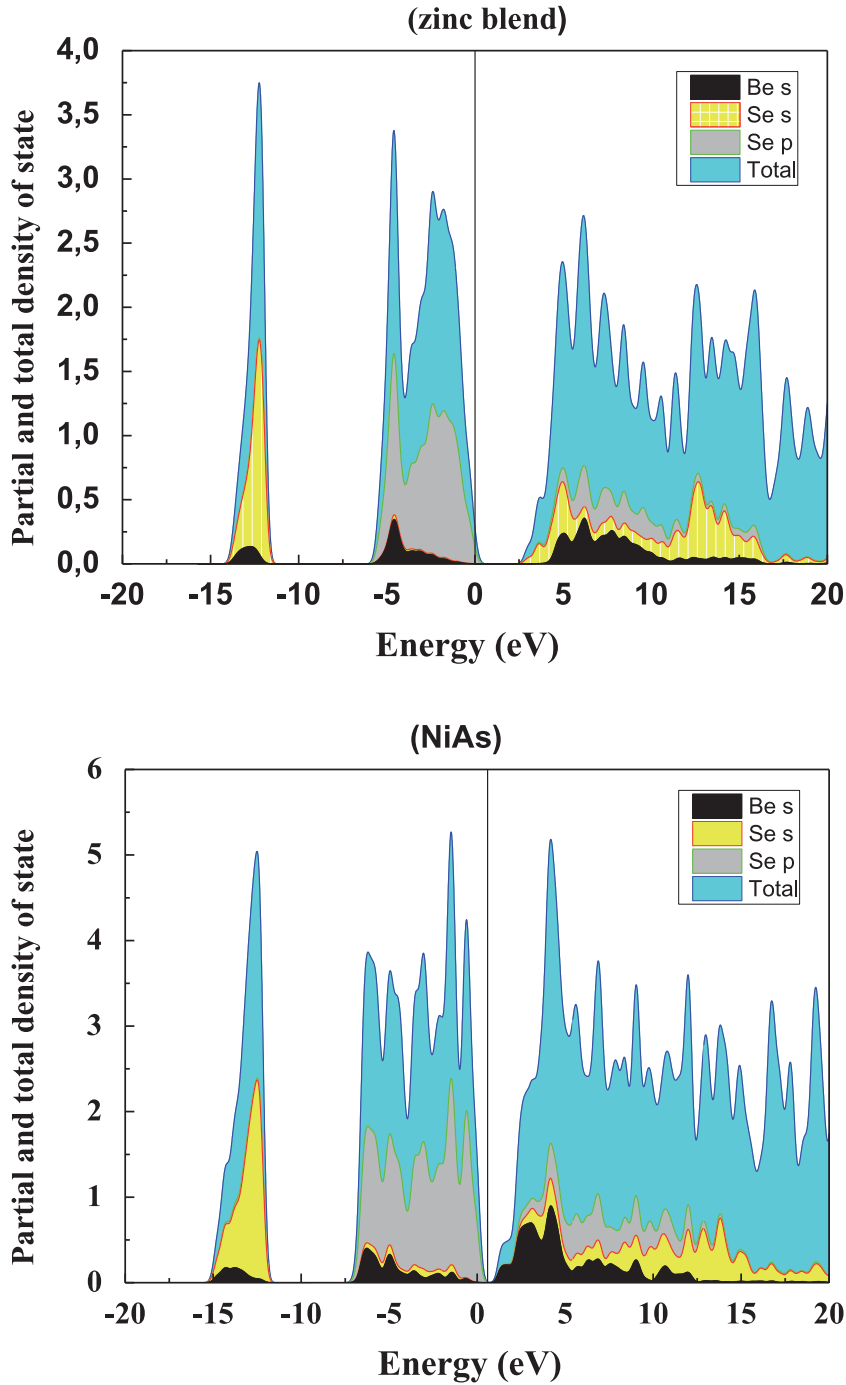


**Figure 6.**  
 Total and partial densities of states.

{longitudinal acoustic (LA)} and transverse optical (TO) {transverse acoustic (TA)} modes and confirm the dynamical stability of BeSe. The frequency  $16.06 \text{ cm}^{-1}$  ( $198 \text{ cm}^{-1}$ ) separates optical (acoustic) longitudinal and transversal branches. The maximum of longitudinal optical phonons is at X point. **Figure 8** shows the effect of pressure on phonon frequencies  $\omega_{LO}$  and  $\omega_{TO}$  of BeSe. The equilibrium values of  $\omega_{LO}$  and  $\omega_{TO}$  at  $\Gamma$  point are  $537 \text{ cm}^{-1}$  and  $471 \text{ cm}^{-1}$ .

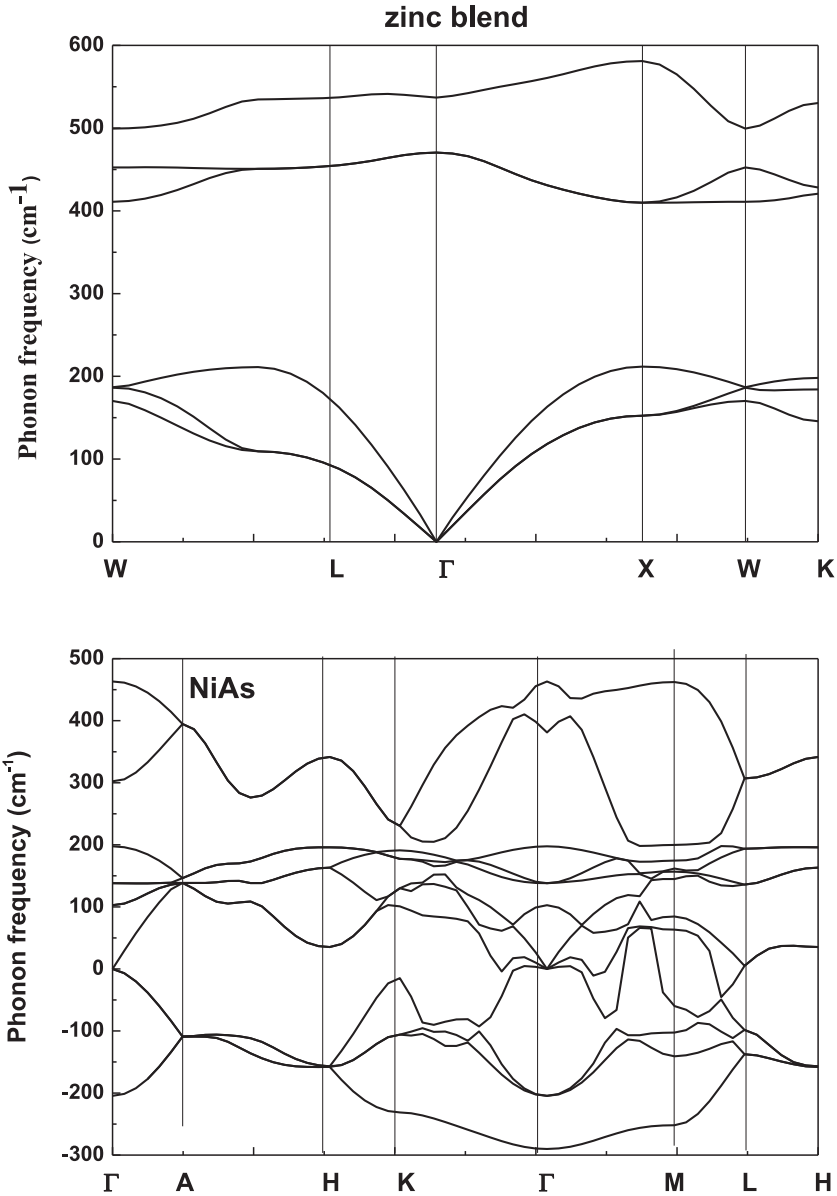
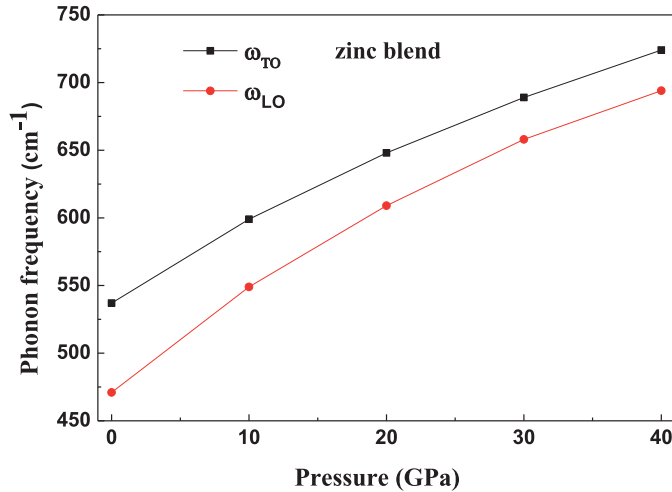


Figure 7.  
The phonon dispersion curves.

### 3.5 Optical parameters

#### 3.5.1 Loss function

We plot in **Figure 9** the loss function spectra versus wavelength for BeSe in zinc blend and NiAs structures. The high-loss region has a wavelength ranging from 42 nm to 90 nm. The low-loss function has a wavelength range less than 40 nm and greater than 90 nm. The maximum loss function reaches the value of 4.84% (4.49%) at 60.32 nm (57.25 nm) in the zinc blend (NiAs) structure. There is no loss in the ultraviolet and visible light domain.



**Figure 8.**  
*The phonon frequency versus pressure at  $\Gamma$  point.*

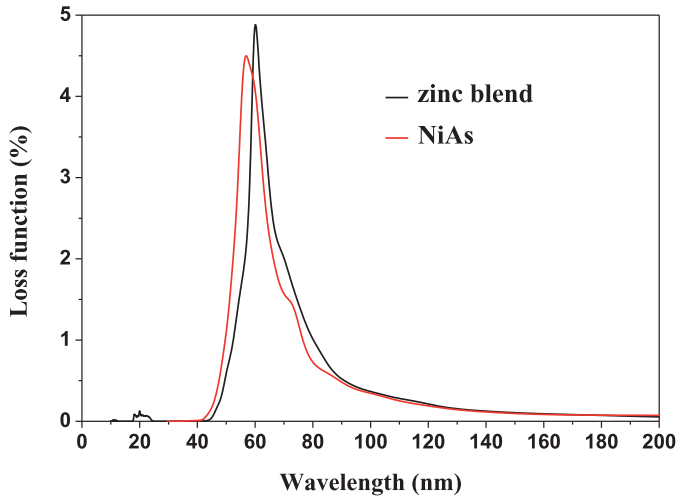


**Figure 9.**  
*The loss function versus wavelength.*

### 3.5.2 Optical absorption

We applied a smearing value of 0.1 to obtain more distinguishable absorbance peaks. We attribute the absorption peaks as depicted in **Figure 10** to the photo transition energies from the maximum valence band to the minimum conduction band under ultraviolet light irradiation. BeSe absorbs a maximum of ultraviolet light  $331,971 \text{ cm}^{-1}$  ( $335,643 \text{ cm}^{-1}$ ) at wavelength 163.6 nm (163 nm) in zinc blend (NiAs) structure, shows narrow indirect bandgap, then it is a good candidate for photocatalysis in the ultraviolet light domain (120–400 nm).

### 3.5.3 Optical reflectivity

The reflectivity estimates the amount of incident light on the surface of photocatalytic material. The reflectivity of BeSe, as shown in **Figure 11**, starts at 0.007

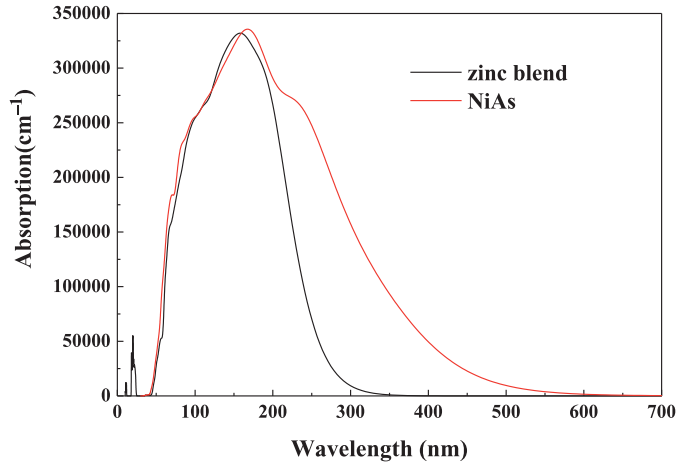


**Figure 10.**  
The absorption versus wavelength.

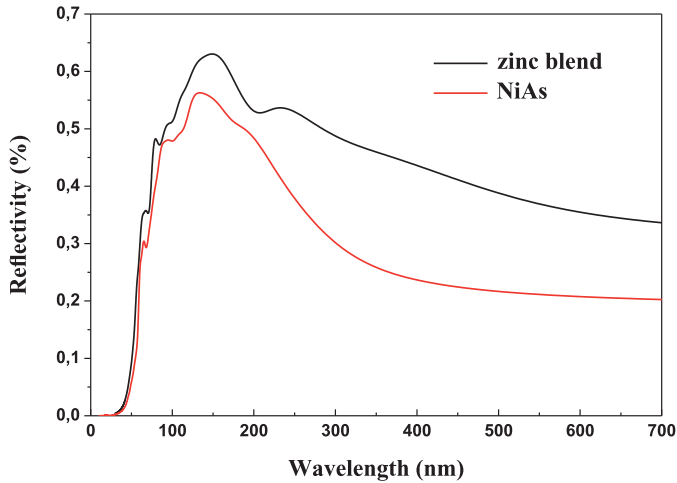


**Figure 11.**  
The reflectivity versus wavelength.

and corresponds to a wavelength around 33 nm. It reaches a maximum value 0.63% (0.56%) at 149 nm (136.5 nm) in zinc blend (NiAs) structure. The reflectivity in the ultraviolet light domain (120 nm–400 nm) is 0.63% (0.56%) in zinc blend (NiAs) structure. While in the visible light (400 nm–800 nm), it is 0.43% (0.23%) for zinc blend (NiAs) phase.

#### 4. Conclusion

We study BeSe in zinc blend and NiAs phases using GGA-PBE, LDA, and HSE hybrid. BeSe is a good candidate for photocatalysis material. We estimate the lattice parameters, shear modulus, Young's modulus, Poisson's ratio, average sound velocities, and Debye temperature. The maximum absorption at ultraviolet light is  $331,971 \text{ cm}^{-1}$  ( $335,643 \text{ cm}^{-1}$ ) in zinc blend (NiAs) structure. We perform transverse and longitudinal optical phonon frequencies  $\omega_{\text{TO}}$  and  $\omega_{\text{LO}}$  at  $\Gamma$  point. A frequency gap

of  $16.06 \text{ cm}^{-1}$  ( $198 \text{ cm}^{-1}$ ) in zinc blend structure separates longitudinal and transversal optical (acoustic) branches. The reflectivity in the ultraviolet light domain is 0.63% (0.56%) in zinc blend (NiAs) structure. While in the visible light, the reflectivity is 0.43% (0.23%) for the zinc blend (NiAs) phase.

## Author details

Mohamed Amine Ghebouli<sup>1\*</sup> and Brahim Ghebouli<sup>2</sup>


1 Faculty of Technology, Department of Chemistry, University of Mohamed Boudiaf, M'sila, Algeria

2 Laboratory of Studies Surfaces and Interfaces of Solids Materials, Faculty of Science, Department of Physics, University Ferhat Abbas of Setif 1, Algeria

\*Address all correspondence to: [mohamedamine.ghebouli@univ-msila.dz](mailto:mohamedamine.ghebouli@univ-msila.dz)

## IntechOpen

---

© 2022 The Author(s). Licensee IntechOpen. This chapter is distributed under the terms of the Creative Commons Attribution License (<http://creativecommons.org/licenses/by/3.0>), which permits unrestricted use, distribution, and reproduction in any medium, provided the original work is properly cited. 

## References

- [1] Ghebouli MA, Ghebouli B, Chihi T, Fatmi M. Study of structural, elastic, electronic, dynamical and optical properties of beryllium selenide (BeSe) semiconductor in zinc blend and NiAs phases. *Physica B Condensed Matter*. 2021;**610**(1):412858. DOI: 10.1016/j.physb.2021.412858
- [2] González-Díaz M, Rodríguez-Hernández P, Munõz A. Elastic constants and electronic structure of beryllium chalcogenides BeS, BeSe, and BeTe from first-principles calculations. *Physical Review B*. 1997;**55**(21):14043
- [3] Srivastava GP, Tütüncü HM, Günhan N. First-principles studies of structural, electronic, and dynamical properties of Be chalcogenides. *Physical Review B*. 2004;**70**:085206
- [4] Yim W, Dismukes J, Stofko E, Paff R. Synthesis and some properties of BeTe, BeSe and BeS. *Journal of Physics and Chemistry of Solids*. 1972;**33**:501-505
- [5] Bouhafis B, Aourag H, Ferhat M, Certier M. Competition between the ionic and covalent character in the series of boron compounds BP, BAs, and BSb. *Phys J. Condensed Matter*. 1999;**11**(30): 5781
- [6] Khenata R, Bouhemadou A, Hichour M, Baltache H, Rached D, Rérat M. Elastic and optical properties of BeS, BeSe and BeTe under pressure. *Solid State Electronics*. 2006;**50**(7-8): 1382-1388
- [7] Pandey R, Sivaraman S. Spectroscopic properties of defects in alkaline-earth sulfides. *Journal of Physics and Chemistry of Solids*. 1991;**52**(1):211-225
- [8] Asano S, Yamashita N, Nakao Y. Luminescence of the  $\text{Pb}^{2+}$ -Ion Dimer Center in CaS and CaSe Phosphors. *Physica Status Solidi*. 1978;**89**(2):663-673
- [9] Nakanishi Y, Ito T, Hatanaka Y, Shimaoka G. Preparation and luminescent properties of SrSe: Ce thin films. *Applied Surface Science*. 1992;**66**:515
- [10] Segall MD, Lindan PJD, Probert MJ, Pickard CJ, Hasnip PJ, Clark SJ, et al. First-principles simulation: Ideas, illustrations and the CASTEP code. *Journal of Physics: Condensed Matter*. 2002;**14**(11):2717-2744
- [11] Monkhorst HJ, Pack JD. Special points for Brillouin-zone integrations. *Physical Review B*. 1976;**13**(12):5188
- [12] Perdew JP, Burke K, Ernzerhof M. Generalized gradient approximation made simple. *Physical Review Letters*. 1996;**77**(18):3865
- [13] Goedecker S, Teter M, Hutter J. Separable dual-space Gaussian pseudopotentials. *Physical Review B*. 1996;**54**(3):1703
- [14] Fischer TH, Almlof J. General methods for geometry and wave function optimization. *The Journal of Physical Chemistry*. 1992;**96**(24): 9768-9774
- [15] Luo H, Ghandehari K, Greene RG, Ruoff AL. Phase transformation of BeSe and BeTe to the NiAs structure at high pressure. *Physical Review B*. 1995; **52**(10):7058
- [16] Kalpana G, Pari G, Mookerjee A, Bhattacharyya AK. *Ab initio* Electronic Band Structure Calculations for Beryllium Chalcogenides. *International Journal of Modern Physics B*. 1998; **12**(19):1975

- [17] Munõz A, Rodriguez-Hernandez P, Mujica A. Ground-state properties and high-pressure phase of beryllium chalcogenides BeSe, BeTe, and BeS. *Physical Review B*. 1996;**54**(17):11861
- [18] Heciri D, Beldi L, Drablia S, Meradji H, Derradji NE, Belkhir H, et al. First-principles elastic constants and electronic structure of beryllium chalcogenides BeS, BeSe and BeTe. *Computational Materials Science*. 2007;**38**(4):609-617
- [19] Bouamama K, Daoud K, Kassali K. Ab initio calculations in the virtual-crystal approximation of the structural and the elastic properties of BeS<sub>x</sub>Se<sub>1-x</sub> alloys under high pressure. *Modelling Simul. Materials Science and Engineering*. 2005;**13**(7):1153
- [20] Dutta R, Alptekin S, Mandal N. Electronic structure, optical properties and the mechanism of the B3–B8 phase transition of BeSe: Insights from hybrid functionals, lattice dynamics and *NPH* molecular dynamics. *Journal of Physics: Condensed Matter*. 2013;**25**(12):125401
- [21] Munjal N, Sharma V, Sharma G, Vyas V, Sharma BK, Lowther JE. Ab-initio study of the electronic and elastic properties of beryllium chalcogenides BeX (X= S, Se and Te). *Physica Scripta*. 2011;**84**(3):035704
- [22] Berghout A, Zaoui A, Hugel J. Fundamental state quantities and high-pressure phase transition in beryllium chalcogenides. *Journal of Physics: Condensed Matter*. 2006;**18**(46):10365-10375
- [23] Okoye CMI. Structural, electronic, and optical properties of beryllium monochalcogenides. *European Physical Journal B*. 2004;**39**(1):5
- [24] Postnikov AV, Pages O, Tite T, Ajjoun M, Hugel J. Examination of Size-Induced Ferroelectric Phase Transitions in Template Synthesized PbTiO<sub>3</sub> Nanotubes and Nanofibers. *Phase Transitions*. 2005;**78**(9–11):219
- [25] Hassan FEH, Akbarzadeh H. Ground state properties and structural phase transition of beryllium chalcogenides. *Computational Materials Science*. 2006;**35**(4):423-431
- [26] Kong F, Jiang G. Phase transition, elastic, thermodynamic properties of zinc-blend BeSe from first-principles. *Physica B*. 2009;**404**(21):3935-3940
- [27] Chattopadhyaya S, Sarkar U, Debnath B, Debbarma M, Ghosh D, Chanda S, et al. Density functional study of structural, elastic, electronic and optical properties of Be<sub>x</sub>Cd<sub>1-x</sub>S, Be<sub>x</sub>Cd<sub>1-x</sub>Se and Be<sub>x</sub>Cd<sub>1-x</sub>Te alloys using FPLAPW approach. *Physica B: Condensed Matter*. 2019;**563**:1-22. DOI: 10.1016/j.physb.2019.03.025
- [28] Cruz WDL, Duaz JA, Mancera L, Takeuchi N, Soto G. Yttrium nitride thin films grown by reactive laser ablation. *Journal of Physics and Chemistry of Solids*. 2003;**64**:2273
- [29] Born M, Hang K. *Dynamical Theory and Experiments I*. Berlin: Springer Verlag Publishers; 1982
- [30] Berning PH, Hass G, Madden RP. Reflectance-increasing coatings for the vacuum ultraviolet and their applications. *Journal of the Optical Society of America*. 1960;**50**(6):586-597
- [31] Rached D, Rabah M, Benkhattou N, Khenata R, Soudini B, Al-Douri Y, et al. First-principle study of structural, electronic and elastic properties of beryllium chalcogenides BeS, BeSe and BeTe. *Computational Materials Science*. 2006;**37**(3):292-299

[32] Sarkar RL, Chatterjee S. Electronic energy bands of BeS, BeSe and BeTe. *Journal of Physics C: Solid State Physics*. 1977;**10**(1):57-62. DOI: 10.1088/0022-3719/10/1/011

[33] Wilmers K, Wethkamp T, Essar N, Cobet C, Richter F, Wagner V, et al. Ellipsometric studies of  $\text{Be}_x\text{Zn}_{1-x}\text{Se}$  between 3 eV and 25 eV. *Physical Review B*. 1999;**59**(15):10071-10075